

## Modelling of an automotive dual mass flywheel

Tobias Mahl \*, Oliver Sawodny \*

\* *Institute for System Dynamics, University of Stuttgart,  
70569 Stuttgart, Germany (e-mail: {tobias.mahl,  
oliver.sawodny}@isys.uni-stuttgart.de)*

**Abstract:** Accurate knowledge of the instantaneous friction torque of an automotive clutch is a key claim while achieving comfortable, automated gearshifts, improving fuel economy or reducing wear. Nevertheless, torque sensors are not commonly used in automotive drive trains because of their additional size and costs. Thus, to estimate the clutch torque, a detailed dynamic model of each component integrated into a clutch system is needed.

In the following, a nonlinear dynamic model of a **Dual Mass Flywheel (DMF)** as autonomous part of a clutch system is presented and verified by test bench data. A DMF is used to reduce the cyclic irregularity of the torque generated by a combustion engine. It is typically assembled between crankshaft and clutch. The level of detail of the modelled DMF dynamics is chosen in a way that a real-time simulation on a car's control unit is feasible. Using the engine speed and the clutch torque as model inputs, the proposed model has the ability to simulate the DMF deflection and therefore the clutch rotational speed. Resulting torques acting on the DMF's primary and secondary mass are reconstructed, too. If both rotation speeds of the DMF masses (the engine and clutch speed) can be measured, this model can also be used to reconstruct the clutch torque.

*Keywords:* Dual Mass Flywheel, DMF, Modelling, Model reduction, Automotive, Drive train, Clutch

### 1. INTRODUCTION

The key function of an automotive clutch system is to accomplish a temporary disengagement of the combustion engine from the gearbox and its following drive train components during standstill or gear changes. To ensure safety and comfort standards, the transition between disengagement and linking has to be continuous. To accomplish this task, a basic clutch system consisting of a DMF with symmetrically arranged arc springs is designed as outlined in Fig. 1.

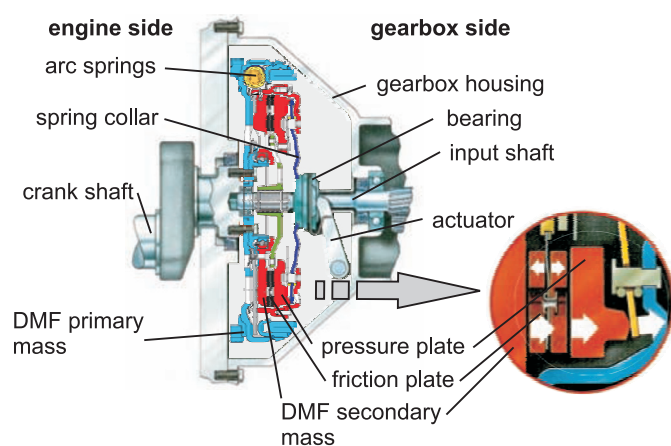


Fig. 1. Automotive clutch system with DMF (origin LUK)

The combustion engine's crank shaft is directly linked to the DMF. The DMF consists of a spring-damper combination attached to two masses (primary and secondary mass). The adjustment between masses and spring-damper is chosen in a way to realize a mechanical lowpass filter reducing the engine torque's cyclic irregularity. The flywheel's secondary mass carries out a key function of the clutch. It deals, together with the pressure plate, as the clutch friction contact rotating with the smoothed engine speed. The friction plate is located between these two plates. It is fixed on the gearbox input shaft. By squeezing the friction plate between the secondary mass and the pressure plate or separating them, the desired clutch torque is generated.

To set up a simulation model of the described clutch configuration, the DMF and the clutch friction dynamics are described, separately. Focusing on the DMF, there exist several references proposing different models for the DMF dynamics. Linear system descriptions are found in Walter et al. (2007) or Walter (2008), whereas nonlinear ones are presented in Lux (2000) or Schaper et al. (2009). Choosing a completely different approach Nicola and Sauer (2006) model the frequency behaviour of the DMF.

In this paper, a dynamic model of an automotive DMF with two symmetrically arranged arc springs is proposed. As the DMF model is part of a clutch model describing the overall clutch system dynamics, the clutch torque is assumed to be known. To obtain the clutch torque, friction models as proposed in Canudas de Wit et al. (1995) or

Dupont et al. (2002) can be used. Beside the clutch torque, the engine speed is required as an additional model input. It is measured with an incremental encoder.

The proposed clutch model is capable to simulate all dominating physical effects of a DMF with symmetrically arranged arc springs. Besides the desired oscillation damping, there are rotational slack, increasing hysteresis over flywheel deflection as well as increasing hysteresis and growing flywheel stiffness over rising engine speed. As the computing complexity is reduced by the proposed model reduction, real-time simulations on a car's control unit are feasible.

The following section presents an overview of the clutch system and the DMF model's system boundaries. Thereafter the DMF model is derived in section 3, which is divided into three parts focusing on modelling, model analysis and model reduction. After the DMF model is introduced, simulation results compared to test bench data are presented in section 4. Concluding remarks are given at the end.

## 2. CLUTCH MODEL OVERVIEW

The examined clutch system (Fig. 1) consists of an automated clutch linked with a DMF. Its simplified mechanical setup is built up as shown in Fig. 2. It consists of two iner-

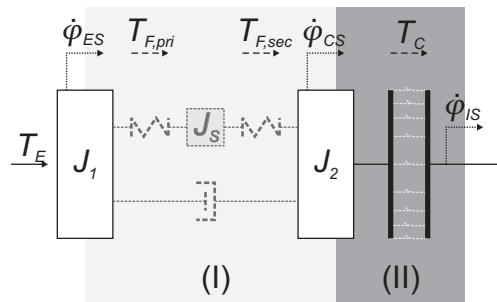


Fig. 2. Schematic clutch model with submodel (I) “DMF model” and submodel (II) “clutch friction model”

tias  $J_1$  and  $J_2$ .  $J_1$  represents the equivalent inertia of the DMF primary side. It includes the inertia of the flywheel's primary mass together with the crankshaft and engine inertias. The rotation speed of the inertia  $J_1$ , named  $\dot{\varphi}_{ES}$  for engine speed, is measured by an incremental encoder.  $J_2$  is the equivalent inertia of the flywheel's secondary mass in addition to the clutch's primary inertia. Its respective rotation speed is called clutch speed  $\dot{\varphi}_{CS}$ . In contrast to the engine speed, the clutch speed is not measured. The last rotating part is the gearbox input shaft with its measured speed  $\dot{\varphi}_{IS}$ . Existing torques are labeled with  $T$  where  $T_E$ ,  $T_{F, pri}$ ,  $T_{F, sec}$  and  $T_C$  are the symbols for the engine, flywheel primary, flywheel secondary and clutch torque.

Using the law of angular momentum conservation, the differential equations of motion for the inertias  $J_1$  and  $J_2$  are

$$J_1 \ddot{\varphi}_{ES} = T_E - T_{F, pri} \quad (1)$$

$$J_2 \ddot{\varphi}_{CS} = T_{F, sec} - T_C. \quad (2)$$

A close description of the flywheel torques  $T_{F, pri}$  and  $T_{F, sec}$  of submodel (I) follows in the next section presenting the

DMF model. As mentioned above, the clutch torque of submodel (II) is assumed to be known. Additionally, it should be mentioned that simulating Eq. (1) is not necessary, as the engine speed is already known by measurements. For the sake of completeness, its equation of motion will be focused further, anyhow.

## 3. DMF MODEL

Schaper et al. (2009) introduced a dynamic DMF model capable to simulate the dominating physical effects of a DMF with symmetrically arranged arc springs. This model consists of a complex sub model for the arc springs and their friction behaviour. As the required step size for a stable forward integration has to be smaller than  $100 \mu s$ , real-time simulations on a car's control unit will exceed the available control unit's computing power. However, the main ideas of this model are the basis for the presented DMF model.

Both masses of the DMF are modelled as inertias having two stoppers each to pick up the arc springs. Each spring gets fragmented into  $N$  segments and  $N - 1$  lumped masses as depicted in Fig. 3. As the DMF is symmetrically,

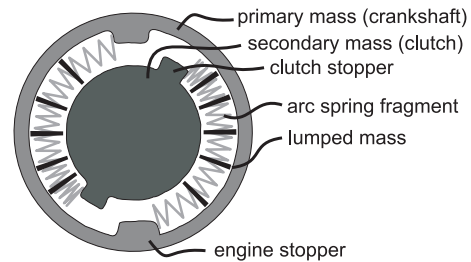


Fig. 3. Simplified sketch of the DMF

only one arc spring is considered in the following. The second one is assumed to behave identically. To transfer torque from one inertia to the other, the spring has to be deflected within the arc spring tunnel and has to touch the stoppers. The damping characteristic of the DMF is caused by sealings between the primary and secondary flywheel mass and by the friction forces resulting from the spring coils sliding through the tunnel. Due to the modelled fragmentation of the arc springs, friction is simulated for the  $N - 1$  lumped masses. By modelling the friction and acceleration forces of the lumped masses, non-homogeneous deflections of the spring segments are reproduced.

### 3.1 Modelling

The following flywheel model assumes the arc spring to be fragmented into two parts ( $N = 2$ ) and therefore one lumped mass. The lumped mass  $m_{S1}$  is symmetrically arranged between both spring segments (S01 and S1N). The characteristics of the spring segments are identically. A schematic sketch of the spring model is depicted in Fig. 4. As the model consists of only one mass, the lumped mass  $m_{S1}$  equals the arc spring mass  $m_S$ . The non-fragmented arc spring characteristic has to be modelled by the two spring segments. In case of a nonlinear spring characteristic, a piecewise linearization of the spring stiffness is used. This results in a spring model where the spring segments

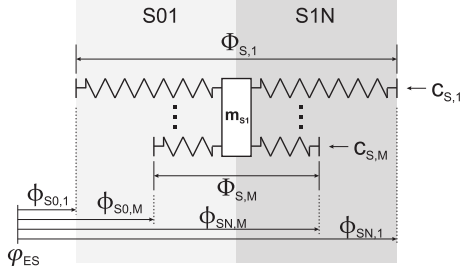


Fig. 4. Sketch of nonlinear spring model

are assumed to be made up of  $M$  parallel arranged linear sub springs with descending nominal lengths. Compared to the piecewise linearized, non-fragmented arc spring stiffnesses  $c_{S,j}$  and related nominal lengths  $\Phi_{S,j}$ , the sub spring stiffnesses and lengths are  $2c_{S,j}$  and  $\frac{1}{2}\Phi_{S,j}$  respectively, with

$$\Phi_{S,1} < \dots < \Phi_{S,M}, \quad j = 1, \dots, M. \quad (3)$$

The sub spring ends which are not connected to the lumped mass are free. Its positions are labelled with  $\Phi_{S0,j}$  for the first and  $\Phi_{SN,j}$  for the second spring segment.

Using this spring model, the resulting schematic setup of the examined DMF is illustrated in Fig. 5. Torsions

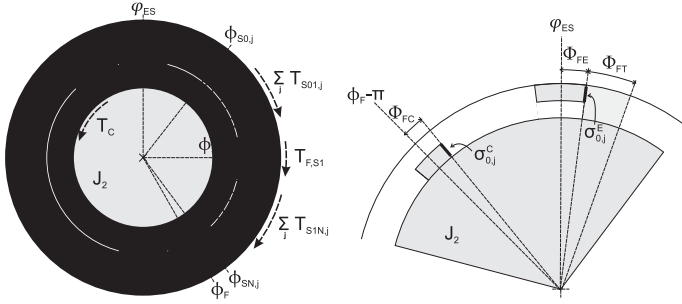


Fig. 5. DMF schematical setup

generated by the sub springs consisting to the first spring segment are labeled with  $T_{S01,j}$  and those consisting to the second with  $T_{S1N,j}$  respectively.  $T_{F,S1}$  denotes the friction torque between the lumped mass and the primary inertia. Relative angular positions are labeled with  $\phi_*$  and refer to the absolute angular position of the primary inertia  $\varphi_{ES}$ .

$$\phi_* = \varphi_* - \varphi_{ES} \quad (4)$$

Those are the relative angular positions  $\phi_{S0,j}$  and  $\phi_{SN,j}$  of the free sub spring ends, the relative deviation of the DMF  $\phi_F$  defined with

$$\phi_F = \pi + \varphi_{CS} - \varphi_{ES} = \pi + \phi_{CS} \quad (5)$$

and the relative position of the lumped mass labeled with  $\phi_{S1}$ . The lumped mass equivalent inertia  $J_{S1}$  is calculated according to the Huygens-Steiner theorem:

$$J_{S1} = m_{S1} \left( \frac{r_{S,i} + r_{S,o}}{2} \right)^2 \quad (6)$$

Here  $r_{S,i}$  and  $r_{S,o}$  are the arc spring inside and outside radius.

The constants  $\Phi_{FE}$  and  $\Phi_{FC}$  are the half widths of the engine and clutch stoppers respectively.

Setting up the dynamic equations for the inertias and using Eq. (1), (2) and (5) results in

$$J_1 \ddot{\varphi}_{ES} = -2 \sum_j \sigma_{0,j}^E T_{S01,j} + 2 \sum_j \sigma_{N,j}^E T_{S1N,j} \dots + T_E - 2T_{F,S1} + T_{Seal} \quad (7)$$

$$J_2 (\ddot{\varphi}_{ES} + \ddot{\phi}_F) = -2 \sum_j \sigma_{0,j}^C T_{S01,j} + 2 \sum_j \sigma_{N,j}^C T_{S1N,j} \dots - T_{Seal} - T_C \quad (8)$$

$$J_{S1} (\ddot{\varphi}_{ES} + \ddot{\phi}_{S1}) = \sum_j T_{S01,j} - \sum_j T_{S1N,j} + T_{F,S1}, \quad (9)$$

with  $T_{Seal}$  representing the sealing friction and damping between the primary and secondary inertia. In the following, Eq. (7)-(9) are described in detail.

*sigma-functions* The  $\sigma^*$ -functions indicate whether the  $j$ -th sub spring touches the first  $\sigma_{0,j}^*$  or second  $\sigma_{N,j}^*$  engine  $\sigma_{*,j}^E$  or clutch  $\sigma_{*,j}^C$  stopper.  $\sigma_*^* = 0$  denotes that the sub spring does not touch the respective stopper, whereas for  $\sigma_*^* = 1$  the sub spring is in contact with the stopper. In addition to a pure switching behaviour between 0 or 1, there is a smooth transition in the region where the sub spring is able to touch two stoppers simultaneously. This transition region, which size is parametrized with  $\Phi_{FT}$ , enables to split up the torque of the sub springs acting on the primary and secondary inertia. The  $\sigma$ -functions are defined as follows:

$$\sigma_{0,j}^E = \begin{cases} 0 & \Phi_{FE} + \Phi_{FT} \leq \phi_{S0,j} \\ \frac{\phi_{S0,j} - \Phi_{FE} - \Phi_{FT}}{\Phi_{FT}} & \Phi_{FE} < \phi_{S0,j} < \Phi_{FE} + \Phi_{FT} \\ 1 & \phi_{S0,j} \leq \Phi_{FE} \end{cases} \quad (10)$$

$$\sigma_{0,j}^C = \begin{cases} 0 & \phi_F + \pi + \Phi_{FC} < \phi_{S0,j} \\ 1 + \frac{\phi_{S0,j} - \Phi_{FE} - \Phi_{FT}}{\Phi_{FT}} & \phi_{S0,j} \leq \phi_F + \pi + \Phi_{FC} \wedge \\ & \dots \phi_{S0,j} < \Phi_{FE} + \Phi_{FT} \\ 1 & \phi_{S0,j} \leq \phi_F + \pi + \Phi_{FC} \wedge \\ & \dots \Phi_{FE} + \Phi_{FT} \leq \phi_{S0,j} \end{cases} \quad (11)$$

$$\sigma_{N,j}^E = \begin{cases} 0 & \phi_{SN,j} \leq \pi - \Phi_{FE} - \Phi_{FT} \\ \frac{\phi_{SN,j} - \pi + \Phi_{FE} + \Phi_{FT}}{\Phi_{FT}} & \pi - \Phi_{FE} - \Phi_{FT} < \phi_{SN,j} \wedge \\ & \dots \phi_{SN,j} < \pi - \Phi_{FE} \\ 1 & \pi - \Phi_{FE} \leq \phi_{SN,j} \end{cases} \quad (12)$$

$$\sigma_{N,j}^C = \begin{cases} 0 & \phi_{SN,j} < \phi_F + \Phi_{FC} \\ 1 - \frac{\phi_{SN,j} - \pi + \Phi_{FE} + \Phi_{FT}}{\Phi_{FT}} & \phi_F + \Phi_{FC} \leq \phi_{SN,j} \wedge \\ & \dots \pi - \Phi_{FC} - \Phi_{FT} < \phi_{SN,j} \\ 1 & \phi_F + \Phi_{FC} \leq \phi_{SN,j} \wedge \\ & \dots \phi_{SN,j} \leq \pi - \Phi_{FC} - \Phi_{FT} \end{cases} \quad (13)$$

*Spring segments* For calculating the sub spring torques it has to be considered that one end of the sub springs is free. Therefore the springs can not be stretched but only be compressed by the stoppers. The positions of the free sub spring ends, named as sub spring boundary conditions, are

$$\phi_{S0,j} = \max \left\{ \Phi_{FE}, \phi_F - \pi + \Phi_{FC}, \phi_{S1} - \frac{\Phi_{S,j}}{2} \right\} \quad (14)$$

$$\phi_{SN,j} = \min \left\{ \pi - \Phi_{FE}, \phi_F - \Phi_{FC}, \phi_{S1} + \frac{\Phi_{S,j}}{2} \right\}. \quad (15)$$

Under consideration of these boundary conditions, the sub spring torques result in

$$T_{S01,j} = -2c_{S,j} \left( \phi_{S1} - \phi_{S0,j} - \frac{\Phi_{S,j}}{2} \right) \quad (16)$$

$$T_{S1N,j} = -2c_{S,j} \left( \phi_{SN,j} - \phi_{S1} - \frac{\Phi_{S,j}}{2} \right). \quad (17)$$

*Lumped mass friction* The hysteresis of the DMF model is mainly evoked by the spring friction. Using the Coulomb friction model it is set up as follows:

$$T_{F,S1} = \begin{cases} -T_{F,S1,max} \text{sign}(\dot{\phi}_{S1}) & \dot{\phi}_{S1} \neq 0 \\ -T_{F,S1,max} \text{sign}(T_{S1,stick}) & \dot{\phi}_{S1} = 0 \wedge T_{F,S1,max} < |T_{S1,stick}| \\ -T_{S1,stick} & \dot{\phi}_{S1} = 0 \wedge T_{F,S1,max} \geq |T_{S1,stick}|. \end{cases} \quad (18)$$

The magnitude of the maximal friction torque  $T_{F,S1,max}$  and the sum of torques acting on the sticking lumped mass  $T_{S1,stick}$  are calculated by:

$$T_{F,S1,max} = \mu r_{S,o} F_{N,S1} \quad (19)$$

$$T_{S1,stick} = \sum_j T_{S01,j} - \sum_j T_{S1N,j} - J_{S1} \ddot{\phi}_{ES}, \quad (20)$$

where  $\mu$  labels the friction coefficient of the arc spring in the arc spring tunnel.  $F_{N,S1}$  represents the normal force pushing the lumped mass to the primary inertia. Three different influences are considered acting radially on the lumped mass and therefore generating the normal force. These are the centrifugal force  $F_{NC,S1}$ , the redirection force  $F_{NR,S1}$  and a bias term  $F_{NB,S1}$ . Therefore  $F_{N,S1}$  results in

$$F_{N,S1} = F_{NC,S1} + F_{NR,S1} + F_{NB,S1}. \quad (21)$$

Last one includes the force which is necessary to bend a uncompressed flat spring into an arc shape.

The centrifugal force acting on the lumped mass is

$$F_{NC,S1} = m_{S1} \left( \frac{r_{S,i} + r_{S,o}}{2} \right) \left( \dot{\phi}_{ES} + \dot{\phi}_{S1} \right)^2. \quad (22)$$

By neglecting the lumped mass relative angular velocity, which is much slower than the engine speed, it can be simplified to

$$F_{NC,S1} \approx m_{S1} \left( \frac{r_{S,i} + r_{S,o}}{2} \right) \dot{\phi}_{ES}^2. \quad (23)$$

The arc spring redirection force depends on the springs deflection and torque transfer. Concentrating the redirection forces of both spring segments to the lumped mass results in

$$F_{NR,S1} = \frac{4}{r_{S,i} + r_{S,o}} \sum_j T_{S01,j} \sin \left( \frac{\phi_{S1} - \phi_{S0,j}}{2} \right) \\ \dots + \frac{4}{r_{S,i} + r_{S,o}} \sum_j T_{S1N,j} \sin \left( \frac{\phi_{SN,j} - \phi_{S1}}{2} \right). \quad (24)$$

The bias term  $F_{NB,S1}$  is a constant force.

*Sealing friction and damping* Further reasons for energy dissipation are sealing friction and damping. To model those energy dissipations, the LuGre friction model (see Canudas de Wit et al. (1995) with Canudas de Wit (1998) and Barahanov and Ortega (2000)) is used.  $T_{Seal}$  is defined as follows:

$$T_{Seal} = \sigma_{0,Seal} \varphi_{B,Seal} + \sigma_{1,Seal} \dot{\varphi}_{B,Seal} + d_{Seal} \dot{\phi}_F \quad (25)$$

$\varphi_{B,Seal}$  is the friction model internal state which can be considered to be a rotational bristle deflection. Using this analogy,  $\sigma_{0,Seal}$  and  $\sigma_{1,Seal}$  are the bristle stiffness and damping respectively, whereas  $d_{Seal}$  is the damping coefficient for the flywheel deflection. The bristle deflection dynamics is

$$\dot{\varphi}_{B,Seal} = \dot{\phi}_F - \frac{\sigma_{0,Seal}}{T_{Seal,max}} \left| \dot{\phi}_F \right| \varphi_{B,Seal}, \quad (26)$$

with a constant maximum sealing friction torque  $T_{Seal,max}$ .

*Parametrization* Tab. 1 contains reasonable parameters for a DMF model, which obviously depend on the type of combustion engine and clutch system installed.

Table 1. Parameters for the presented DMF model

Parameter	Parameter
$J_1 = 0.30 \text{ kg m}^2$	$\Phi_{S,j} = \{2.83, 2.11\} \text{ rad}$
$J_2 = 0.12 \text{ kg m}^2$	$c_{S,j} = \{96.0, 322.3\} \frac{\text{Nm}}{\text{rad}}$
$m_S = 0.40 \text{ kg}$	$\mu = 0.08$
$r_{S,i} = 0.113 \text{ m}$	$\sigma_{0,Seal} = 573 \frac{\text{Nm}}{\text{rad}}$
$r_{S,o} = 0.135 \text{ m}$	$\sigma_{1,Seal} = 1.0 \frac{\text{Nm}\cdot\text{s}}{\text{rad}}$
$\Phi_{FE} = 0.13 \text{ rad}$	$d_{Seal} = 2.8 \frac{\text{Nm}\cdot\text{s}}{\text{rad}}$
$\Phi_{FC} = 0.10 \text{ rad}$	$T_{Seal,max} = 5.0 \text{ Nm}$
$\Phi_{FT} = 0.03 \text{ rad}$	$F_{NB,S1} = 290 \text{ N}$

### 3.2 Model analysis

Computing power is still a limiting factor for simulations on a car's control unit. In order to find a reasonable simulation step size  $h$ , the model dynamics are analyzed. Having a linear model, a good indication for the step size is obtained by calculating the model time constants  $T$  gained by the model eigenvalues  $\lambda$ . Choosing the step size ten times faster than the shortest time constant results in

$$h = \frac{1}{10} \min \{T\} = \frac{1}{10} \min \left\{ \frac{1}{|\text{Re}(\lambda)|}, \frac{2\pi}{|\text{Im}(\lambda)|} \right\}. \quad (27)$$

Doing so will lead to simulation results capable to reproduce the modelled dynamics accurately<sup>1</sup>.  $\text{Re}(\lambda)$  and  $\text{Im}(\lambda)$  are the eigenvalue real and imaginary parts respectively. To apply this method for nonlinear models, a model linearization is needed.

*Eigenvalues of the linearized model* The basis for calculating the eigenvalues of the linearized DMF model are Eq. (8) and (9). Assuming the engine speed to be constant and neglecting all friction torques, the equations of motion result in

$$J_2 \ddot{\phi}_F = -2 \sum_j \sigma_{0,j}^C T_{S01,j} + 2 \sum_j \sigma_{N,j}^C T_{S1N,j} - T_C \quad (28)$$

$$J_{S1} \ddot{\phi}_{S1} = \sum_j T_{S01,j} - \sum_j T_{S1N,j}. \quad (29)$$

As a further assumption, the acting clutch torque is positive, constant and its magnitude high enough that all  $M$  sub springs are touching a stopper. This configuration leads to the shortest time constants possible as the arc

<sup>1</sup> This is just a common indication for the step size. Besides the step size, stability and convergence of the simulation are influenced by the system eigenvalues and the used numeric integration method.

spring stiffness is at its maximum. Using this assumption, the  $\sigma$ -functions and sub spring boundary conditions are

$$\sigma_{0,j}^C = 0, \quad \sigma_{N,j}^C = 1 \quad (30)$$

$$\phi_{S0,j} = \Phi_{FE}, \quad \phi_{S1} = \frac{\phi_F}{2}, \quad \phi_{SN,j} = \phi_F - \Phi_{FC}. \quad (31)$$

Inserting them in Eq. (28) and (29), together with the equations defining the sub spring torques (Eq. (16), (17)), leads to

$$J_2 \ddot{\phi}_F = -2 \sum_j c_{S,j} \phi_F + 4 \sum_j c_{S,j} \left( \Phi_{FC} + \frac{\Phi_{S,j}}{2} \right) - T_C \quad (32)$$

$$J_{S1} \ddot{\phi}_{S1} = -4 \sum_j c_{S,j} \phi_{S1} + 2 \sum_j c_{S,j} \phi_F. \quad (33)$$

These second order differential equations, representing undamped oscillators, consist of the following eigenvalues:

$$\lambda_{1,2}^{J_2} = 0 \pm i \sqrt{\frac{2 \sum_j c_{S,j}}{J_2}}, \quad \lambda_{1,2}^{J_{S1}} = 0 \pm i \sqrt{\frac{4 \sum_j c_{S,j}}{J_{S1}}} \quad (34)$$

Converting the eigenvalues to time constants  $T$ , which represent the duration of a whole oscillation, and inserting the DMF model parameters results in

$$T_{J_2} = \frac{2\pi}{\sqrt{\frac{2 \sum_j c_{S,j}}{J_2}}} \approx 75 \text{ ms}, \quad T_{J_{S1}} = \frac{2\pi}{\sqrt{\frac{4 \sum_j c_{S,j}}{J_{S1}}}} \approx 10 \text{ ms}. \quad (35)$$

By analysing the eigenvalues of both equations of motion, it is seen that the dynamics representing the spring motion is about 7.5 times faster than these representing the secondary flywheel mass motion. Using Eq. (27), the recommended, maximal sample time will be 1 ms.

### 3.3 Model reduction

As the spring motion dynamics is much faster than the secondary flywheel's inertia dynamics, the quasi-steady-state approximation is applied to the faster dynamics. This model reduction technique assumes that the lumped spring mass reaches its equilibrium in a time scale much faster than the step size. Therefore, only its steady-state position, but not the overall dynamics, influences the simulation results. Using this model reduction, the recommended step size rises to 7.5 ms without losing simulation accuracy significantly.

*Quasi-steady-state approximation* To compute the lumped mass steady-state position  $\phi_{S1,ss}$ , Eq. (9) is utilized with  $\ddot{\phi}_{S1}$  and  $\dot{\phi}_{S1}$  appointed to zero.

$$J_{S1} \ddot{\phi}_{ES} = \sum_j T_{S01,j,ss} - \sum_j T_{S1N,j,ss} + T_{F,S1} \quad (36)$$

Each variable recomputed after the steady-state calculation is indicated by the additional index  $_{ss}$ . If there is no additional index added, this variable either does not depend on the lumped mass position or the position before steady-state calculation is used. Solving Eq. (36) for  $\phi_{S1,ss}$  leads to the wanted equilibrium. Due to the lumped mass friction, a case distinction is necessary.

- Case I:  $T_{F,S1,max} \geq |T_{S1,stick}|$
- Case II:  $T_{F,S1,max} < |T_{S1,stick}|$

In the case where the maximal friction torque is larger or equal the sum of torques acting on the sticking lumped mass, the mass will not move.

$$\phi_{S1,ss} = \phi_{S1} \quad (37)$$

Therefore it rests in its position which equals the steady-state position and no further calculations are necessary.

In the second case, the mass will move. As this movement changes the sub spring boundary conditions, uncompressed sub springs may get compressed or the other way round. Without extensive computations, the sub spring steady-state configuration is not predictable. One way to get to the unique equilibrium is to compute the steady-state position with each sub spring configuration possible and selecting the physically right one afterwards. This results in the following  $5M - 2$  proposed equilibria  $\tilde{\phi}_{S1,ss,i}$

$$\begin{aligned} \tilde{\phi}_{S1,ss,i} = & \frac{\sum_j (\tilde{\sigma}_{0,j,ss,i}^E + \tilde{\sigma}_{0,j,ss,i}^C) \left( \max \{ \Phi_{FE}, \phi_F - \pi + \Phi_{FC} \} + \frac{\Phi_{S,j}}{2} \right) c_{S,j}}{\sum_j (\tilde{\sigma}_{0,j,ss,i}^E + \tilde{\sigma}_{0,j,ss,i}^C) c_{S,j} + \sum_j (\tilde{\sigma}_{N,j,ss,i}^E + \tilde{\sigma}_{N,j,ss,i}^C) c_{S,j}} c_{S,j} \\ & \dots + \frac{\sum_j (\tilde{\sigma}_{N,j,ss,i}^E + \tilde{\sigma}_{N,j,ss,i}^C) \left( \min \{ \pi - \Phi_{FE}, \phi_F - \Phi_{FC} \} - \frac{\Phi_{S,j}}{2} \right) c_{S,j}}{\sum_j (\tilde{\sigma}_{0,j,ss,i}^E + \tilde{\sigma}_{0,j,ss,i}^C) c_{S,j} + \sum_j (\tilde{\sigma}_{N,j,ss,i}^E + \tilde{\sigma}_{N,j,ss,i}^C) c_{S,j}} c_{S,j} \\ & \dots + \frac{T_{F,S1} - J_{S1} \ddot{\phi}_{ES}}{2 \sum_j (\tilde{\sigma}_{0,j,ss,i}^E + \tilde{\sigma}_{0,j,ss,i}^C) c_{S,j} + 2 \sum_j (\tilde{\sigma}_{N,j,ss,i}^E + \tilde{\sigma}_{N,j,ss,i}^C) c_{S,j}}, \end{aligned} \quad (38)$$

with

$$\tilde{\sigma}_{0,j,ss,i}^E + \tilde{\sigma}_{0,j,ss,i}^C \in \{0, 1\}, \quad \tilde{\sigma}_{N,j,ss,i}^E + \tilde{\sigma}_{N,j,ss,i}^C \in \{0, 1\} \quad (39)$$

and

$$\Phi_{S,1} < \dots < \Phi_{S,M}, \quad j = 1, \dots, M, \quad i = 1, \dots, 5M - 2. \quad (40)$$

Here,  $\tilde{\sigma}_{*,i}^*$  are the proposed sub spring boundary conditions. To select the physically right equilibrium, each proposed steady-state position has to be inserted in Eq. (10)-(13), which leads to  $5M - 2$  different results  $\hat{\sigma}_{*,ss,i}^*$ , representing possible stiffness configurations. The correct and unique equilibrium  $I$ , which is part of the proposed equilibria, satisfies the two following conditions:

$$\hat{\sigma}_{0,j,ss,I}^E + \hat{\sigma}_{0,j,ss,I}^C = \tilde{\sigma}_{0,j,ss,I}^E + \tilde{\sigma}_{0,j,ss,I}^C \quad (41)$$

$$\hat{\sigma}_{N,j,ss,I}^E + \hat{\sigma}_{N,j,ss,I}^C = \tilde{\sigma}_{N,j,ss,I}^E + \tilde{\sigma}_{N,j,ss,I}^C \quad (42)$$

With

$$j = 1, \dots, M, \quad I \in i \quad i = 1, \dots, 5M - 2. \quad (43)$$

Therefore the lumped mass steady-state position and the steady-state sub spring boundary conditions result in

$$\phi_{S1,ss} = \tilde{\phi}_{S1,ss,I}, \quad \sigma_{*,j,ss}^* = \hat{\sigma}_{*,j,ss,I}^*. \quad (44)$$

Inserting  $\phi_{S1,ss}$  in Eq. (14)-(17) leads to the steady-state positions of the free sub spring ends  $\varphi_{S*,j,ss}$  and steady-state torques  $T_{S*,j,ss}$ , needed to compute Eq. (36).

*Example* This short example presents how to appoint the  $5M - 2$  possible sub spring configurations. Choosing  $M$  to two results in the truth table Tab. 2, displaying all configurations possible by combinational logic. Physically possible configurations are numbered. The others are marked with x. Physically impossible solutions are these where a sub spring with higher number of the same spring fragment touches a stopper without all other sub springs with lower numbers of the same fragment touching the stopper, too. This is because of the sub springs are ordered by

Table 2. Possible sub spring configurations

	i	*	1	x	2	3	4	x	5	x	x	x	x	6	7	x	8
$\sigma_{0,1,ss,i}^E + \sigma_{0,1,ss,i}^C$	0	1	0	1	0	1	0	1	0	1	0	1	0	1	0	1	1
$\sigma_{0,2,ss,i}^E + \sigma_{0,2,ss,i}^C$	0	0	1	1	0	0	1	1	0	0	1	1	0	0	1	1	1
$\sigma_{N,1,ss,i}^E + \sigma_{N,1,ss,i}^C$	0	0	0	0	1	1	1	1	0	0	0	0	0	1	1	1	1
$\sigma_{N,2,ss,i}^E + \sigma_{N,2,ss,i}^C$	0	0	0	0	0	0	0	0	1	1	1	1	1	1	1	1	1

falling nominal length. Only one exception exists which is physically possible but is no correct solution for any steady-state. The case where no sub spring is touching any stopper, marked with \*, can never be a steady-state solution for case II, where the lumped mass moves at the beginning.

4. MODEL VALIDATION

To show the capability of the proposed DMF model, three simulations are presented. The first one is a quasi-stationary deflection simulation with rising DMF rotation speed. The second one simulates a damped oscillation of the DMF to validate its dynamics. The last one describes a combustion engine start and vehicle drive away simulation. Measurement data is recorded on a clutch and gearbox test bench using electric motors to simulate the combustion engine and the vehicle torque during driving. The test bench configuration is displayed in Fig. 6.

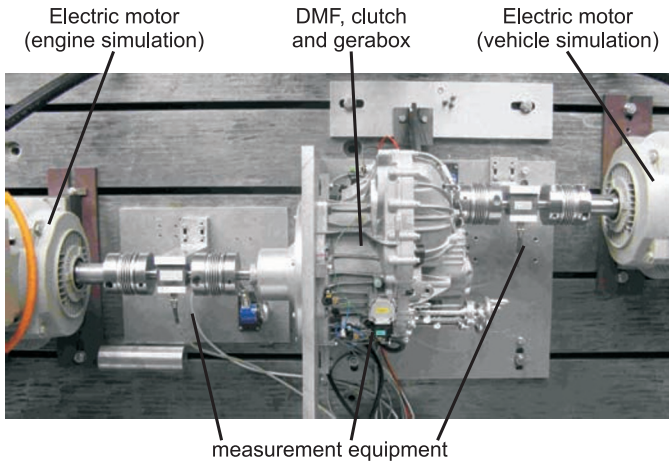


Fig. 6. Clutch and gearbox test bench configuration

For simulation the whole DMF model including Eq. (1) and (2) is used. The measured engine torque and the simulated clutch torque serve as model inputs. To get the clutch torque, a clutch friction model is necessary. The used one bases on the elasto-plastic friction model (see Dupont et al. (2000), Dupont et al. (2002)) having the input shaft speed and the clutch normal force as further inputs. As the clutch is completely closed during the first two experiments, there does not occur any clutch slip. Therefore the clutch model degenerates to a stiff spring-damper combination with linear deflection and damping characteristic in these experiments. For model validation, the simulated speed and rotational position of the engine shaft  $\omega_{ES,sim}$  and  $\varphi_{ES,sim}$  are compared with its respective measurement data  $\omega_{ES,meas}$  and  $\varphi_{ES,meas}$ .

*Quasi-stationary deflection* The first simulation presents (see Fig. 7) the resulting stationary DMF deflection  $\phi_F$  over engine torque for different gearbox input shaft speeds. Therefore the engine torque is specified as a slowly rising

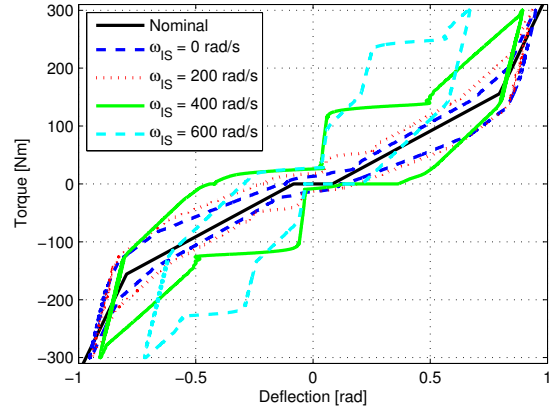


Fig. 7. Deflection simulation with varying input shaft speed

and falling ramp between  $\pm 300$  Nm and the input shaft speed is chosen to be constant. It can clearly be seen that the dominating physical effects of a DMF, which are rotational slack, increasing hysteresis over flywheel deflection as well as growing stiffness over rising engine speed, are simulated by the DMF model.

*Damped oscillation* The DMF dynamics is validated by a second simulation. It shows the progress of oscillation after an abrupt change of engine torque. Therefore the input shaft is blocked against rotation. As depicted in Fig. 8,

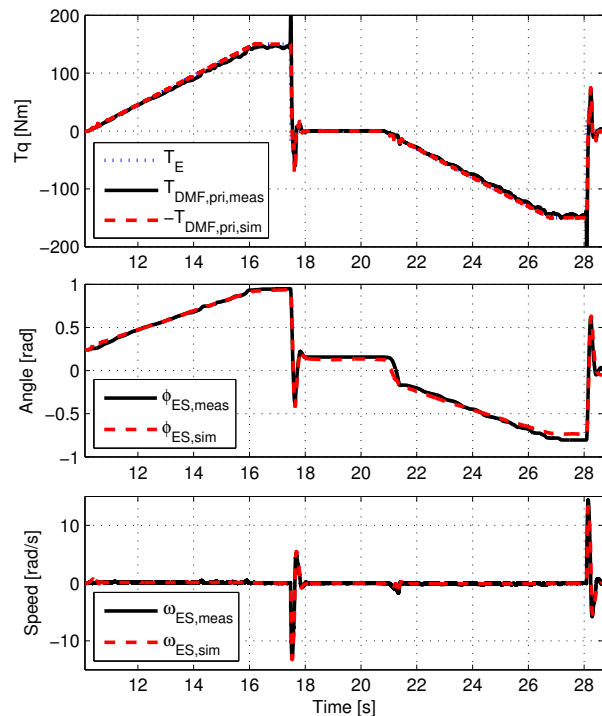


Fig. 8. DMF oscillation experiment

the engine torque is increased up to 150 Nm. After reaching the desired torque, the electric motor is switched off. This results in a damped oscillation of the engine inertia evoked by the prestressed DMF. After the oscillation is abated, the same experiment is executed in opposite direction.

It can be seen, that the simulated engine shaft speed and position matches the measured one very well. This includes the section where the DMF gets deflected, as well as the region where the oscillation takes place. At  $t \approx 21$  s, a fast change of the engine shaft position occurs without any significant variation of the engine torque. Here the modelled and actual rotational slack of the DMF can be compared. A zoomed plot of the oscillation region is presented in Fig. 9.

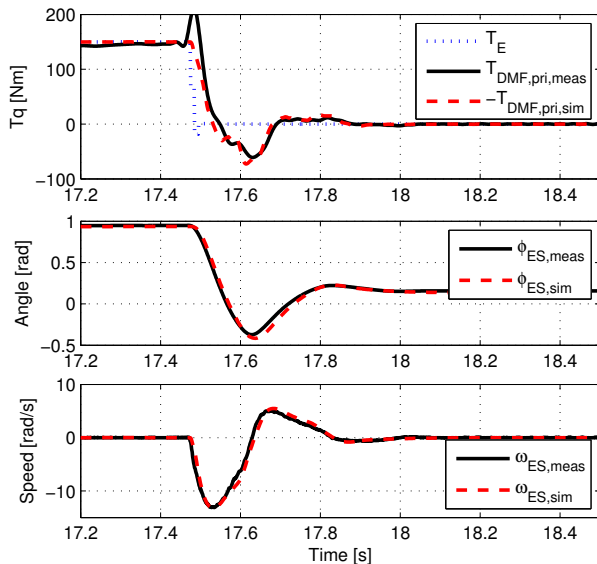


Fig. 9. Zoomed section of DMF oscillation experiment

*Engine start and drive away* The last validation experiment is displayed in Fig. 10. It shows simulation results of a combustion engine start and vehicle drive away simulation. For simulation, the engine torque is composed of two parts.

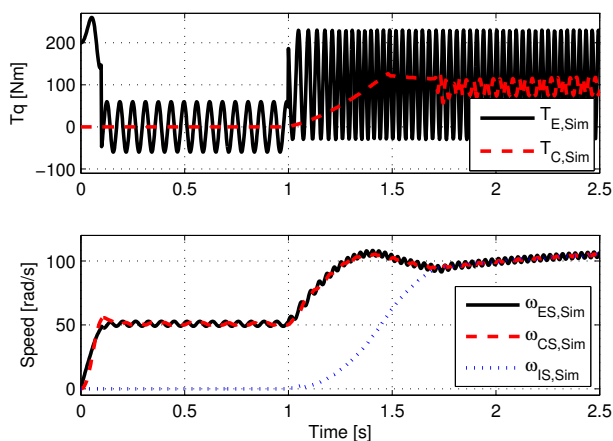


Fig. 10. Engine start and vehicle drive away simulation

Part one is the engine's mean torque. It is overlaid by an unbiased oscillation which is part two. The oscillation frequency depends on the actual engine speed and its amplitude rises with increasing engine's mean torque. After engine start and reaching idle speed the clutch gets closed ( $t = 1$  s). As soon as the clutch begins to transmit torque, the vehicle starts to move.

Comparing engine speed with clutch speed, it can be seen that the clutch speed oscillation is smoothed by the DMF. This results in a reduced oscillation amplitude of the transmitted clutch torque after synchronisation ( $t > 1.7$  s) which is much lower than the initial combustion engine's torque irregularity.

## 5. CONCLUSION

The DMF dynamics have been modelled by a nonlinear system. It consists of the equations of motion of both DMF masses described by the law of angular momentum conservation. To simulate the torque acting on the DMF masses, a detailed model of the DMF arc springs and its frictional behaviour have been presented. As the spring model dynamics consist of time constants much faster than those of the DMF masses, a model reduction is advantageous. To reduce the model complexity, the quasi-steady-state approximation has been used for the arc spring dynamics. The reduced model is capable to describe all dominating physical effects of a DMF. Simulations on a car's control unit are feasible as the computational complexity is low. To validate the DMF model, simulation results have been compared with test bench data.

## REFERENCES

- Barahanov, N. and Ortega, R. (2000). Necessary and sufficient conditions for passivity of the lugre friction model. *IEEE Transactions on Automatic Control*, 45(4), 830–832. doi:10.1109/9.847131.
- Canudas de Wit, C. (1998). Comments on a new model for control of systems with friction. *IEEE Transactions on Automatic Control*, 43(8), 1189–1190.
- Canudas de Wit, C., Olsson, H., Astrom, K.J., and Lischinsky, P. (1995). A new model for control of systems with friction. *IEEE Transactions on Automatic Control*, 40(3), 419–425. doi:10.1109/9.376053.
- Dupont, P., Armstrong, B., and Hayward, V. (2000). Elasto-plastic friction model: contact compliance and stiction. In *Proc. American Control Conference the 2000*, volume 2, 1072–1077 vol.2. doi: 10.1109/ACC.2000.876665.
- Dupont, P., Hayward, V., Armstrong, B., and Altpeter, F. (2002). Single state elastoplastic friction models. *IEEE Transactions on Automatic Control*, 47(5), 787–792. doi: 10.1109/TAC.2002.1000274.
- Lux, R. (2000). *Ganzheitliche Antriebsstrangentwicklung durch Integration von Simulation und Versuch*. Ph.D. thesis, Universität Karlsruhe.
- Nicola, A. and Sauer, B. (2006). Experimentelle ermittlung des dynamikverhaltens torsionselastischer antriebsselemente. *ATZ*, 02, 124 – 130.
- Schaper, U., Sawodny, O., Mahl, T., and Blessing, U. (2009). Modeling and torque estimation of an automotive dual mass flywheel. In *American Control Conference, 2009. ACC '09.*, 1207–1212. doi: 10.1109/ACC.2009.5160136.
- Walter, A. (2008). *Regelung und Diagnose von Fahrzeug-Antriebssträngen mit Zweimassenschwungrad*. Ph.D. thesis, Universität Karlsruhe.
- Walter, A., Brummund, S., Merz, B., Kiencke, U., Jones, S., and Winkler, T. (2007). Estimation of the instantaneous engine torque for vehicles with dual mass flywheel (dmf). In *Advances in Automotive Control*, volume 5.